Tumor-Infiltrating Regulatory T-cell Accumulation in the Tumor Microenvironment Is Mediated by IL33/ST2 Signaling

Jimin Son[1,2], Jae-Won Cho[2,3], Hyo Jin Park[1,2], Jihyun Moon[1,2], Seyeon Park[1,2], Hoyoung Lee[4], Jeewon Lee[4], Gamin Kim[5], Su-Myeong Park[5], Sergio A. Lira[6], Andrew N. Mckenzie[7], Hye Young Kim[8], Cheol Yong Choi[9], Yong Taik Lim[10], Seong Yong Park[11], Hye Ryun Kim[5], Su-Hyung Park[4,12], Eui-Cheol Shin[4,12], Insuk Lee[2,3,13], and Sang-Jun Ha[1,2]

ABSTRACT

Regulatory T cells (Treg) are enriched in the tumor microenvironment (TME) and suppress antitumor immunity; however, the molecular mechanism underlying the accumulation of Tregs in the TME is poorly understood. In various tumor models, tumor-infiltrating Tregs were highly enriched in the TME and had significantly higher expression of immune checkpoint molecules. To characterize tumor-infiltrating Tregs, we performed bulk RNA sequencing (RNA-seq) and found that proliferation-related genes, immune suppression–related genes, and cytokine/chemokine receptor genes were upregulated in tumor-infiltrating Tregs compared with tumor-infiltrating $CD4^{+}Foxp3^{-}$ conventional T cells or splenic Tregs from the same tumor-bearing mice. Single-cell RNA-seq and T-cell receptor sequencing also revealed active proliferation of tumor infiltrating Tregs by clonal expansion. One of these genes, ST2, an IL33 receptor, was identified as a potential factor driving Treg accumulation in the TME. Indeed, IL33-directed ST2 signaling induced the preferential proliferation of tumor-infiltrating Tregs and enhanced tumor progression, whereas genetic deletion of ST2 in Tregs limited their TME accumulation and delayed tumor growth. These data demonstrated the IL33/ST2 axis in Tregs as one of the critical pathways for the preferential accumulation of Tregs in the TME and suggests that the IL33/ST2 axis may be a potential therapeutic target for cancer immunotherapy.

Introduction

Regulatory T cells (Treg) are a prominent immunosuppressive cell type that associates with tumor progression (1, 2). Increased Tregs in the tumor microenvironment (TME) impair antitumor immunity (3). Treg ablation in DEREG mice delays tumor growth and, in some cases, induces complete tumor clearance (2, 4). However, Treg depletion is often accompanied by life-threatening autoimmunity (5). Therefore, distinguishing and selectively targeting tumor-infiltrating Tregs is required for effective and safe cancer immunotherapy.

Three potential sources for Tregs in the TME are trafficking from the periphery, *in situ* conversion from conventional T cells (Tconv), and local proliferation (6). Certain chemokines facilitate Treg recruitment into the TME (7–9). The chemokine receptor, CCR8, is a unique characteristic of tumor-infiltrating Tregs in colorectal cancers, non–small cell lung cancers (NSCLC), and breast cancers (10, 11). Tumor-infiltrating Tregs are generated in TME through the TGFβ-dependent conversion of Tconvs (12). Tregs proliferate in response to IL2 and TGFβ in the TME (5), yet the contribution of these signals has not yet been measured experimentally in the TME.

IL33 is normally released after tissue stress or damage to function as an alarmin. During inflammation and cancer, IL33 exerts multiple regulatory functions on Th2 cells, ILC2s, and Tregs, all which express the unique receptor of IL33, ST2 (13). ST2 is regulated via a positive feedback loop in response to IL33 (14). IL33 facilitates the expansion of adipose Tregs or colonic Tregs (15, 16). However, the role of IL33/ST2 signaling in tumor-infiltrating Tregs is not clear, although IL33 in the TME is protumorigenic (17).

Here, we showed that Tregs preferentially accumulated in the TME of various tumor models. We found that tumor-infiltrating Tregs had a distinct transcriptional feature involved in proliferation and were clonally expanded. ST2 was significantly upregulated in tumor-infiltrating Tregs and IL33 promoted the selective proliferation of ST2-expressing tumor-infiltrating Tregs *in vitro* and *in vivo*. Conversely, genetic deficiency of ST2 in Tregs led to their limited accumulation in the TME and *in vivo* blockade of ST2 delayed tumor growth. These data advance our understanding of tumor-infiltrating

[1]Department of Biochemistry, College of Life Science & Biotechnology, Yonsei University, Seoul, Republic of Korea. [2]Brain Korea 21 (BK21) PLUS Program, Initiative for Biological Functions & Systems, Yonsei University, Seoul, Republic of Korea. [3]Department of Biotechnology, College of Life Science & Biotechnology, Yonsei University, Seoul, Republic of Korea. [4]Biomedical Science and Engineering Interdisciplinary Program, KAIST, Daejeon, Republic of Korea. [5]Division of Medical Oncology, Department of Internal Medicine, Yonsei Cancer Center, Yonsei University College of Medicine, Seoul, Republic of Korea. [6]Precision Immunology Institute, Icahn School of Medicine at Mount Sinai, New York, New York. [7]Medical Research Council Laboratory of Molecular Biology, Cambridge, United Kingdom. [8]Department of Biomedical Sciences, Seoul National University College of Medicine, Seoul, Republic of Korea. [9]Department of Biological Sciences, Sungkyunkwan University, Suwon, Gyeonggi-do, Republic of Korea. [10]SKKU Advanced Institute of Nanotechnology (SAINT), Department of Nano Engineering, School of Chemical Engineering, Sungkyunkwan University, Suwon, Gyeonggi-do, Republic of Korea. [11]Department of Thoracic and Cardiovascular Surgery, Yonsei University College of Medicine, Seoul, Republic of Korea. [12]Graduate School of Medical Science and Engineering, KAIST, Daejeon, Republic of Korea. [13]Department of Biomedical Systems Informatics, Yonsei University College of Medicine, Seoul, Republic of Korea.

Note: Supplementary data for this article are available at Cancer Immunology Research Online (http://cancerimmunolres.aacrjournals.org/).

J. Son and J.-W. Cho contributed equally to this article.

Corresponding Authors: Sang-Jun Ha, Yonsei University, Seoul 03722, Korea. Phone: 822-2123-2696; Fax: 822-362-9897; E-mail: sjha@yonsei.ac.kr; and Insuk Lee. Phone: 82-2-2123-5559; Fax: 82-2-362-7265; E-mail: insuklee@yonsei.ac.kr

Cancer Immunol Res 2020;8:1393–406

doi: 10.1158/2326-6066.CIR-19-0828

Tregs, suggesting an opportunity for therapeutic targeting of Tregs in the TME.

Materials and Methods

Mice

Five- to eight-week-old female C57BL/6, C57BL/6-CD45.1, BALB/c, C57BL/6-Foxp3-GFP, and Rag2$^{-/-}$ mice were purchased from the Jackson Laboratory. ST2-knockout (KO) mice were a generous gift from Dr. Andrew N. Mckenzie (Medical Research Council Laboratory of Molecular Biology, Cambridge, United Kingdom). All mice were maintained in a specific pathogen-free facility in accordance with Institutional Animal Care and Use Committee (IACUC) guidelines at Yonsei University (Seoul, Korea). Animal experiments were approved by the IACUC of Yonsei University (approval number: 201507–356–02, oversight number: 201710–410–06).

Tumor models

The murine lung adenocarcinoma cell line TC-1, Lewis lung carcinoma cell line LLC1, and colon carcinoma cell line CT26 were purchased from the ATCC in 2010 and cultured two passages before injection. Tumor cells were tested yearly for *Mycoplasma* contamination using the e-Myco Mycoplasma PCR Detection Kit (iNtRON Biotechnology) and reauthentication was not performed in the past years. C57BL/6 mice were injected subcutaneously on the right flank or intravenously into the tail vein with 5×10^5 TC-1 or LLC1 tumor cells diluted in 500 μL of PBS. BALB/c mice were injected subcutaneously on the right flank or intravenously into the tail vein with 5×10^5 CT26 tumor cells. At 3 weeks following tumor cell inoculation, tumor-bearing mice and age-matched normal mice were sacrificed. The spleen, lung, and tumor were harvested and processed into single cells.

To study whether ST2 deficiency can affect tumor-infiltrating Treg accumulation, the lung tumors were harvested from TC-1 tumor–bearing wild-type (WT) or ST2-deficient mice on day 21 following tumor cell inoculation. The number of tumor nodules on left upper lobe of the lung were counted using a hemocytometer.

For treatment with neutralizing antibody, TC-1–tumor bearing WT mice were established as described above and each mouse was treated intravenously with 100 μg of anti-ST2 antibody (DIH4, BioLegend) or isotype control antibody (BioLegend) per dose every 2 days, which started on day 5, and sacrificed on day 15.

Isolation of lymphocytes from the tissues

At 3 weeks following tumor inoculation, the spleen and tumor from tumor-bearing mice and the spleen and lung from normal mice were harvested and processed into single cells. Tumors and lung tissues were chopped to 1-mm^3 pieces and digested in RPMI medium supplemented with 10% FBS (Gibco), 1% penicillin–streptomycin, 1% Collagenase IV (Worthington Biochemical Corp.), and 0.01% DNase (Sigma Aldrich) for 20 minutes at 37°C. The fragments were dissociated and passed through a 70-μm strainer. Lymphocytes were collected from the interphase of the 44% and 67% Percoll (Sigma Aldrich) layers after density-gradient centrifugation.

Antibodies and flow cytometry

Cells were stained with the following fluorochrome-conjugated antibodies in FACS buffer (PBS containing 2% FBS): murine CD4 (RM4–5), PD-1 (29F.1A12), CD103 (2E7), Ly5.1 (A20), CCR4 (2G12), and CCR8 (SA214G2; BioLegend); CD25 (PC61.5), CTLA-4 (UC10–4B9), GATA3 (TWAJ), Foxp3 (FJK-16s), Ly5.2 (104), and ST2 (RMST2–33; eBiosciences); GITR (DTA-1), BrdU (3D4), Ki67 (B56), Ly-6C (AL-21), KLRG1 (2F1; BD Biosciences); TIM-3 (215008), and CCR2 (475031; R&D Systems); CCR5 (HM-CCR5; Thermo Fisher Scientific). For ST2 detection, cells were incubated with anti-ST2 biotin for 1 hour at 37°C, washed twice with FACS buffer, and then incubated with streptavidin-APC (Thermo Fisher Scientific, S868) during surface staining. The intracellular staining was conducted using Foxp3 Fixation/Permeabilization solution (Thermo Fisher Scientific, 00–5523–00). For staining cells with antibodies against chemokine receptors, cells were incubated with anti-CCR2, anti-CCR4, and anti-CCR8 antibody for 30 minutes at room temperature and anti-CCR5 antibody for 1 hour at 37°C and then washed twice with FACS buffer before surface staining. To remove dead cell population, the Live/Dead Fixable Dead Cell Stain Kit (Thermo Fisher Scientific, L10119) was used during the staining procedures. Flow cytometry was performed using the FACSCanto II (BD Biosciences) and CytoFLEX LX (Beckman Coulter Life Sciences). Data were analyzed using FlowJo software (Treestar).

Mouse bulk RNA-sequencing and gene-set enrichment analysis

A total of 5×10^5 TC-1 cells were intravenously injected into the tail vein of mice. The spleen and tumor from tumor-bearing mice and spleen from normal mice were harvested at 3 weeks following tumor inoculation. CD4$^+$ T cells were enriched using a CD4$^+$ T Cell Isolation Kit by negative selection (Miltenyi Biotec, 130–104–454) followed by manufacturer's protocol. Pure CD4$^+$GFP$^+$ Treg and CD4$^+$GFP$^-$ Tconv populations were obtained through sorting using a FACSAria II (BD Biosciences). The purity of isolated Tregs was greater than 95%. Total RNA was extracted using a QIAGEN RNeasy Plus Micro Kit (Qiagen, 74034) according to the manufacturer's methods. Libraries were prepared using an Illumina TruSeq Stranded mRNA Library Prep Kit (Illumina, 20020594) and sequenced using an Illumina NextSeq500. For the RNA sequencing (RNA-seq) data analyses, we aligned short sequence reads to the mouse reference genome (UCSC mm10; ref. 18) using STAR-2.5.2a (19) followed by quantification using the FeatureCounts (20). We selected candidate genes based on the consensus of four different combinations of read alignment and quantification/differential analysis methods: (i) Tophat v2.0.13 and Cuffdiff v2.2.0, (ii) STAR and EdgeR, (iii) STAR and DESeq2, and (iv) Kallisto 0.42.5 and DESeq2.

Gene-set enrichment analysis (GSEA) was performed for using gene sets representing immunosuppression, proliferation, chemotaxis, and apoptosis pathways. A total of 325, 853, 122, and 465 genes (Supplementary Table S1) were compiled from 159, 164, 39, and 113 gene ontology (GO) biological process terms (Supplementary Table S2) relevant to immunosuppression, proliferation, chemotaxis, and apoptosis categories, respectively. Only genes annotated by GO, evidence of experimental or literature curated data, were used.

Single-cell RNA-seq and T-cell receptor sequencing analysis

CD4$^+$ T cells were enriched from pooled lung tissues of normal mice ($n = 10$) and pooled TC-1 tumors of tumor-bearing mice ($n = 7$) as described previously. Single-cell sequencing libraries were prepared by using Chromium 10x Genomics platform with a V(D)J Enrichment Kit and 5′ Library & Gel Bead Kit (10x Genomics, PN-1000005, PN-1000006) according to the manufacturer's instructions. The single-cell suspensions of live CD4$^+$ T cells sorted by FACSAria II were diluted in nuclease-free water and then combined with Single Cell 5′ Gel Beads, a master mix, and Partitioning Oil on Chromium Chip A, found in the aforementioned kit. RNA transcripts were uniquely barcoded and reverse-transcribed within nanoliter-scale droplets

containing uniquely barcoded beads. 10x barcoded full-length cDNA were then pooled and enriched via PCR. For V(D)J Enriched Library, the enriched cDNA pool was amplified using primers specific to T-cell receptor (TCR). For 5′ Gene Expression (GEX) library, the cDNA pool went through an end repair process, A-tailing, adaptor ligation, and sample index PCR. Both libraries for single-cell RNA-seq (scRNA-seq) and single-cell TCR sequencing (scTCR-seq) were sequenced using HiSeqX platform (Illumina).

Cell Ranger analysis pipeline (v3.1.0) was applied to the raw sequencing data to obtain a gene count and a clonotype information for each cell. Using Seurat version 3.1 pipeline, we filtered out cells based on proportion of mitochondrial genes and feature count. Next, we selected cells that have both scRNA-seq and scTCR-seq data. Raw expression data was log normalized with scale factor of 10,000. Downstream analysis was conducted on the basis of top 2,000 highly variable genes only. To avoid batch effect, we integrated sequencing data from normal and tumor samples using default data integration pipeline of Seurat v3.1. Dimension reduction and clustering analysis were performed by UMAP and Louvain clustering (dimension: 50 and resolution: 0.21) algorithms available from Seurat package.

Compositional changes between cellular group of single clonal TCR (singlet) and that of multiple clonal TCR (multiplet) were assessed on the basis of the Pearson residual: $d_{ij} = \frac{n_{ij} - m_{ij}}{\sqrt{m_{ij}}}$, where i and j represent a group (singlet or multiplet) and cell subsets, respectively, and n and m are the observed cell number and the expected cell count, respectively. The significance of the compositional changes was evaluated on the basis of χ^2 test. The results of compositional analysis were summarized as a mosaic plot.

BrdU

For BrdU labeling, TC-1 tumor–bearing mice and normal mice were injected intraperitoneally (i.p.) with 2 mg BrdU (Sigma) for 6 consecutive days prior to sacrifice. BrdU incorporation was detected by intracellular staining using the BrdU Flow Kit (BD Biosciences, 559619) according to the manufacturer's methods.

Apoptosis assay

To detect apoptosis, cells were stained with Annexin V and 7-AAD using an Annexin V Apoptosis Detection Kit (BD Biosciences, 556547) according to the manufacturer's methods.

Multistep candidate gene filtering procedure

Mouse coding genes from the Consensus Coding sequence (CCDS) database (21) were filtered for cell membrane and cell surface genes annotated in Swiss-Prot (22) and for external side of plasma membrane genes annotated in GO (23) with GO evidence code of IDA, IPI, IMP, IGI, IEP, TAS, and EXP. Next, 2,613 genes passed the filtration step were further filtered for tumor-bearing mice-TM Treg–specific differentially expressed genes (DEG) compared with five other cellular and tissue contexts, resulting in five sets of DEGs: tumor-bearing mice-TM Tregs versus tumor-bearing mice-TM Tconvs [fold change (FC) > 4], tumor-bearing mice-SP Tregs (FC > 2), tumor-bearing mice-SP Tconvs (FC > 2), normal mice-SP Tregs (FC > 2), or normal mice-SP Tconvs (FC > 2) with $P < 0.05$. For highly conservative candidate selection, we used DEGs by consensus of four different analysis pipelines as described above for each of the five comparisons. The intersection of the five DEG sets resulted in 37 genes. We excluded the genes that had low expression, assuming an expression value of lower than 10% of the CD4 (a marker for $CD4^+$ T cells) expression level might be insufficient for the therapeutic effect. The expression profile of the 17 genes that passed the low expression filtration across other immune cell types was examined using the Gene Skyline data browser of Immgen Project (24). The filtering of genes that were highly expressed in other immune cell types resulted in only three candidate genes. Foxp3 was used as reference gene because it is a specific marker for Tregs, having an expression level of approximately 700 in $CD4^+$ memory T cells. Thus, we applied a strict threshold expression level of 500.

Multiplex immunofluorescence staining

Naïve lung and tumor on days 8 and 12 following inoculation were harvested. Sections (4.5 μm) of tissues were cut from formalin-fixed paraffin-embedded (FFPE) blocks and dried for at least 1 hour in 60°C dry incubator. The sections were dewaxed using xylene, then followed by multiplex immunofluorescence staining with a Leica Bond Rx Automated Stainer (Leica Biosystems).

Briefly, the slides were baked for 30 minutes and dewaxed with Leica Bond Dewax solution (Leica Biosystems, AR9222), followed by antigen retrieval with Bond Epitope Retrieval 2 (Leica Biosystems, AR9640) in a pH 9.0 solution for 30 minutes. Then, the slides were incubated with first primary antibody for CD45 (clone 30-F11, Thermo Fisher Scientific, 14–0451–81) for 30 minutes. Visualization of CD45 was accomplished using Opal 570 TSA Plus for 10 minutes, after which the slide was treated with Bond Epitope Retrieval 1 (Leica Biosystems, AR9961) for 20 minutes to remove bound antibodies before the next step in the sequence. Then, the sections were stained with CD31 (polyclonal, Abcam, ab124432, Opal 520), IL33 (Clone 396118, R&D Systems, MAB3626, Opal 690), and PDPN (polyclonal, Abcam, ab109059, Opal 620), sequentially. Nuclei were subsequently visualized with DAPI (Akoya Biosciences, FP1490), and the section was coverslipped using HIGHDEF IHC fluoromount (Enzo Life Sciences, ADI-950–260–0025). The slides were scanned using the Vectra Polaris Automated Quantitative Pathology Imaging System (Akoya Biosciences) and images were analyzed using the inform 2.4 software and TIBCO Spotfire (Akoya Biosciences).

ELISA

At each time point, lungs were collected, weighed, and homogenized in 1 mL of DMEM supplemented with 1% FBS. After homogenate being centrifuged, the supernatant was analyzed for IL33 production using Mouse IL33 DuoSet ELISA (R&D Systems, DY3626–05) according to the manufacturer's protocol.

Expansion of Tregs *in vitro* using various recombinant cytokines

For *in vitro* proliferation assays, single-cell suspensions from the tumor of TC-1 tumor–bearing mice at 21 days following tumor inoculation were enriched for $CD4^+$ cells using the MagniSort Mouse CD4 T Cell Enrichment Kit (Thermo Fisher Scientific, 8804–6821). A total of 10^5 $CD4^+$ T cells labeled with CellTrace-Violet dye (CTV, Thermo Fisher Scientific) were resuspended in expansion buffer (RPMI, 10% FBS, 1% penicillin/streptomycin). CTV-labeled $CD4^+$ T cells were left unstimulated or stimulated with 0.5 μg/mL soluble anti-CD3/CD28 (BD Biosciences) supplemented with 10 ng/mL rhIL33 (PeproTech) and cultured for 3 days.

For blocking of ST2 on Tregs, CTV-labeled $CD4^+$ T cells were incubated for 1 hour with 10 μg/mL of anti-ST2 antibody (R&D Systems) or isotype control antibody (BioXCell) at 4°C, washed twice, and stimulated with 0.5 μg/mL soluble anti-CD3/CD28 supplemented with 10 ng/mL rhIL33 for 3 days.

Expansion of Tregs *in vivo* using recombinant IL33

To expand Tregs *in vivo*, TC-1 tumor–bearing mice either WT mice or ST2-deficient mice were intraperitoneally injected with 2 μg rmIL33 (BioLegend) diluted in 200 μL of PBS on day 4 or days 4, 7, and 10 following tumor inoculation and sacrificed on day 13. The number of tumor nodules were counted as described above.

Functional assay of IL33-treated tumor-infiltrating Tregs

For *in vitro* suppression assay, TC-1 tumor–bearing mice were intraperitoneally treated with either PBS or rmIL33 in the manner as described above and sacrificed on day 13 following tumor inoculation. We isolated the Tregs from PBS-treated tumor-bearing mice and IL33-treated tumor-bearing mice using $CD4^+CD25^+$ Regulatory T Cell Isolation Kit (Miltenyi Biotec, 130–091–041). We also harvested the spleen from naïve mouse, isolated $CD8^+$ T cells with $CD8a^+$ T Cell Isolation Kit (Miltenyi Biotec, 130–104–075), and labeled them with CTV dye. Then, PBS-treated Tregs (PBS Treg) or IL33-treated Tregs (IL33 Treg) were cocultured with $CD8^+$ T cells as ratio of 1:1 or 1:3 supplemented with Dynabeads Mouse T-Activator CD3/CD28 for T-Cell Expansion and Activation (Gibco, 11452D) for 72 hours.

Adoptive transfer

To study the mechanism for the accumulation of tumor-infiltrating Tregs, $CD4^+CD25^+$ Tregs were isolated from the spleen of either WT or ST2-KO mice using a $CD4^+CD25^+$ Regulatory T Cell Isolation Kit (Miltenyi Biotec). An equal number of WT and ST2-KO Tregs (1.5×10^5 cells per group) were cotransferred or seperately transferred intravenously into the tail vein of $Rag2^{-/-}$ mice along with 1.2×10^6 WT $CD8^+$ T cells (500 μL of PBS). Two weeks after the transfer, the $Rag2^{-/-}$ mice were injected intravenously into the tail vein with 5×10^5 TC-1 tumor cells. At day 21 following tumor cell inoculation, tumors were isolated form each mouse for counting of tumor nodules on left upper lobe of the lung and the two different populations of donor Tregs in the tissues were analyzed.

Statistical analysis

Experimental data were analyzed using GraphPad Prism software (GraphPad). Significant difference between two groups was analyzed by two-tailed unpaired Student *t* test. For comparison between more than two groups, one-way ANOVA was used with Bonferroni *post hoc* test. Results are presented as mean ± SEM. The difference between two experimental groups with a *P* value less than 0.05 was considered statistically significant. The Kolmogorov–Smirnov two-tailed test was performed to analyze the statistical significance in empirical cumulative distribution functions (ECDF). The statistical significance of difference between two Pearson correlation coefficient (PCC) distributions was tested by the Wilcoxon rank-sum test.

Data availability

All original bulk RNA-seq data and scRNA-seq data including TCR-seq data were deposited in the NCBI's Gene Expression Omnibus (GEO) database (GEO: GSE120280, GSE152022).

Results

Tregs were significantly enriched and phenotypically activated in the TME

To examine the population of Tregs at the tumor site, we took advantage of various tumor models in which mice were subcutaneously or intravenously injected with murine TC-1 lung adenocarcinoma, LLC1 Lewis lung carcinoma, or CT26 colon carcinoma cells. Under homeostatic conditions, Tregs represent 5% to 10% of $CD4^+$ T cells in the lung and 10% to 15% in the spleen. Regardless of tumor model or route of tumor cell injection, we found the frequencies of Tregs in tumor-bearing mice significantly increased, up to a maximum of 40%, in the TME compared with those in the spleen (**Fig. 1A** and **B**; Supplementary Fig. S1A). Both frequency and absolute number of Tregs in the tumor lung increased compared with those in the normal lung (**Fig. 1B**).

Analysis of the expression of functional molecules by Tregs in TC-1 lung tumor model, CTLA-4, PD-1, TIM-3, and GITR, demonstrated that tumor-infiltrating Tregs were phenotypically activated, suggesting their enhanced suppressive function (**Fig. 1C** and **D**). Increased PD-1 expression in tumor-infiltrating Tregs was also observed in other tumor models (Supplementary Fig. S1B and S1C). We found the monocyte/macrophage and endothelial cell differentiation antigen, Ly-6C, was downregulated in tumor-infiltrating Tregs (**Fig. 1E**). As Ly-6C downregulation is under the control of TCR signaling (25), enrichment of Ly-$6C^{lo}$ Tregs may be due to sustained exposure to tumor or self-antigens present in the TME. These results suggested the TME instigated the accumulation of tumor-infiltrating Tregs with distinguishable phenotype.

Immune-related genes are upregulated in tumor-infiltrating Tregs

To identify the molecular mechanisms leading to tumor-infiltrating Treg accumulation, transcriptional profiles of Tregs and Tconvs derived from either tumor of tumor-bearing mice or spleen of normal mice and tumor-bearing mice were compared using RNA-seq analysis (**Fig. 2A**). Comparison of our mouse RNA-seq data to that of human tumor-infiltrating Tregs from patients with NSCLC (10) indicated the transcriptional profile of tumor-infiltrating Tregs correlates each other (Supplementary Fig. S2). Activated Treg genes for which we had already determined protein expression (CTLA-4 (*Ctla4*), GITR (*Tnfrsf18*), TIM-3 (*Havcr2*), and PD-1 (*Pdcd1*)) were upregulated in tumor-infiltrating Tregs. Tumor-infiltrating Tregs also highly expressed genes associated with immunosuppressive function including immunosuppressive soluble factors *Il10* and *Gzmb*, ectonucleotidase *Entpd1* (CD39), and coinhibitory receptors *Ctla4, Pdcd1, Havcr2*, and *Tigit*. In addition, the genes for several cytokine and chemokine receptors including *Il1rl1, Ccr2, Ccr4, Ccr5*, and *Ccr8* were upregulated (**Fig. 2B**). Protein expressions of CCR2, CCR5, and CCR8, but not CCR4, were highly upregulated by tumor-infiltrating Tregs in our TC-1 lung cancer model (Supplementary Fig. S3).

GSEA (26) showed genes involved in immunosuppression, proliferation, chemotaxis, and apoptosis were significantly upregulated in tumor-infiltrating Tregs compared to tumor-infiltrating Tconvs and splenic Tregs of tumor-bearing mice (**Fig. 2C**). In addition, the Kolmogorov–Smirnov test revealed a significant enrichment of genes associated with proliferation in tumor-infiltrating T cells compared with splenic T cells of tumor-bearing mice, especially in Tregs rather than Tconvs (**Fig. 2D**). In contrast, the enrichment was not observed in splenic T cells from between tumor-bearing mice and normal mice (Supplementary Fig. S4). Collectively, these data suggested that both enhanced migration and proliferation activity led to the increased population of Tregs in the TME.

Single-cell analysis revealed active proliferation of tumor-infiltrating Tregs

For direct comparison of T cells from lung tumor and normal lung, we conducted scRNA-seq and scTCR-seq for $CD4^+$ T cells from

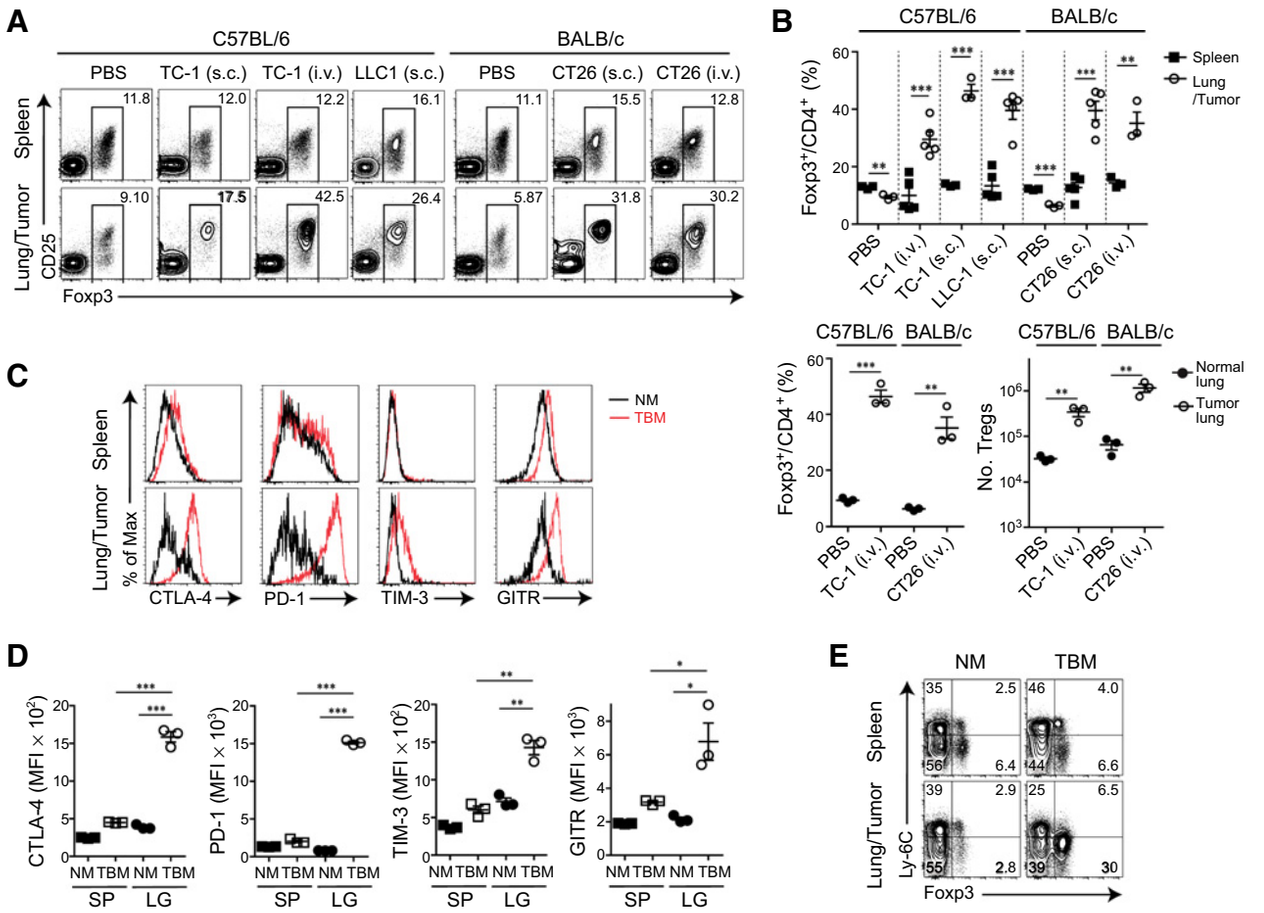

Figure 1.

Tregs accumulated in the TME and expressed activation molecules. **A** and **B,** Representative plots of Treg frequency gated on CD4$^+$ T cells from the tissues of normal mice and tumor-bearing mice with TC-1, LLC1, and CT26 (**A**). Frequency of tumor-infiltrating Tregs or normal lung Tregs compared with splenic Tregs (**B**, top). Frequency (**B**, bottom left) and number (**B**, bottom right) of tumor-infiltrating Tregs compared with normal lung Tregs. i.v., intravenous; s.c., subcutaneous. Representative plots (**C**) and median fluorescence intensity (MFI; **D**) of the indicated molecules by Tregs from the spleen (SP) and lung (LG) of normal mice (NM) and TC-1 tumor–bearing mice (TBM). **E,** Expression of Ly-6C and Foxp3 by CD4$^+$ T cells. Data are representative of three independent experiments. Results are presented as the mean ± SEM and analyzed by two-tailed unpaired Student *t* test (n = 3–5/group; *, $P < 0.05$; **, $P < 0.01$; ***, $P < 0.001$).

TC-1 lung tumor of tumor-bearing mice and those from normal lung of normal mice (**Fig. 3A**). Single-cell transcriptome data from normal and tumor tissue samples were integrated with batch correction by "multi dataset integration" function of Seurat v.3.1 (Supplementary Fig. S5A; ref. 27). Unsupervised clustering of the cells based on transcriptome similarity revealed seven clusters, all which expressed CD4$^+$ T-cell markers for T cells (Supplementary Fig. S5B), representing subsets of CD4$^+$ T cells (Supplementary Fig. S6A). **Figure 3B** shows the transcriptome landscape of CD4$^+$ T cells organized by tissue origin (left; tumor lung or normal lung), by cluster (middle), and by clonality (right; multiplet or singlet). Tregs were annotated by the expression of *Foxp3* and *Il2ra* and the rest of the cells were annotated as Tconvs (Supplementary Fig. S6B). We further examined the profiles of signature genes to characterize the Tconv clusters (Supplementary Fig. S6B and S6C). As a result, cluster 1 showed higher expression of exhaustion markers (*Ctla4, Pdcd1*, and *Tigit*), whereas the rest of the Tconvs showed higher expression of naive signature (*Sell* and *Ccr7*). Therefore, we annotated cluster 1 as exhausted Tconv (exhTconv) and the rest of Tconvs clusters as naïve Tconv (nTconv). For Tregs, we annotated cluster 2 as activated Treg (aTreg) and cluster 5 as resting Treg (rTreg) based on the distribution of clonality (**Fig. 3B**) and the expression of activated Treg signature (*Sell*^{lo}, *Ccr7*^{lo}, *Itgae*^{hi}, *Klrg1*^{hi}; Supplementary Fig. S6B and S6C). As expected, more Tregs were observed in lung tumor than in normal lung. In addition, most of tumor-infiltrating Tregs showed aTreg phenotype, whereas normal lung Tregs seemed to be composed of more rTregs than aTregs (**Fig. 3B**). Treg ratio was much higher in lung tumor than normal lung (**Fig. 3C**), which was consistent with the results from flow cytometric analysis (**Fig. 1B**). In addition, most of the multiple-clonotype Tregs were found in tumor-infiltrating Tregs but not in normal lung Tregs (**Fig. 3B**). As shown in the mosaic plot, which represents the deviation from the expected cell count for each group (singlet or multiplet) for each CD4$^+$ T-cell subset, most of the multiple-clonotype Tregs were enriched in tumor-infiltrating aTregs, whereas there was no multiple-clonotype Tregs in tumor-infiltrating rTregs (**Fig. 3D**). This observation indicated that clonally expanded Tregs were enriched in tumor tissue upon

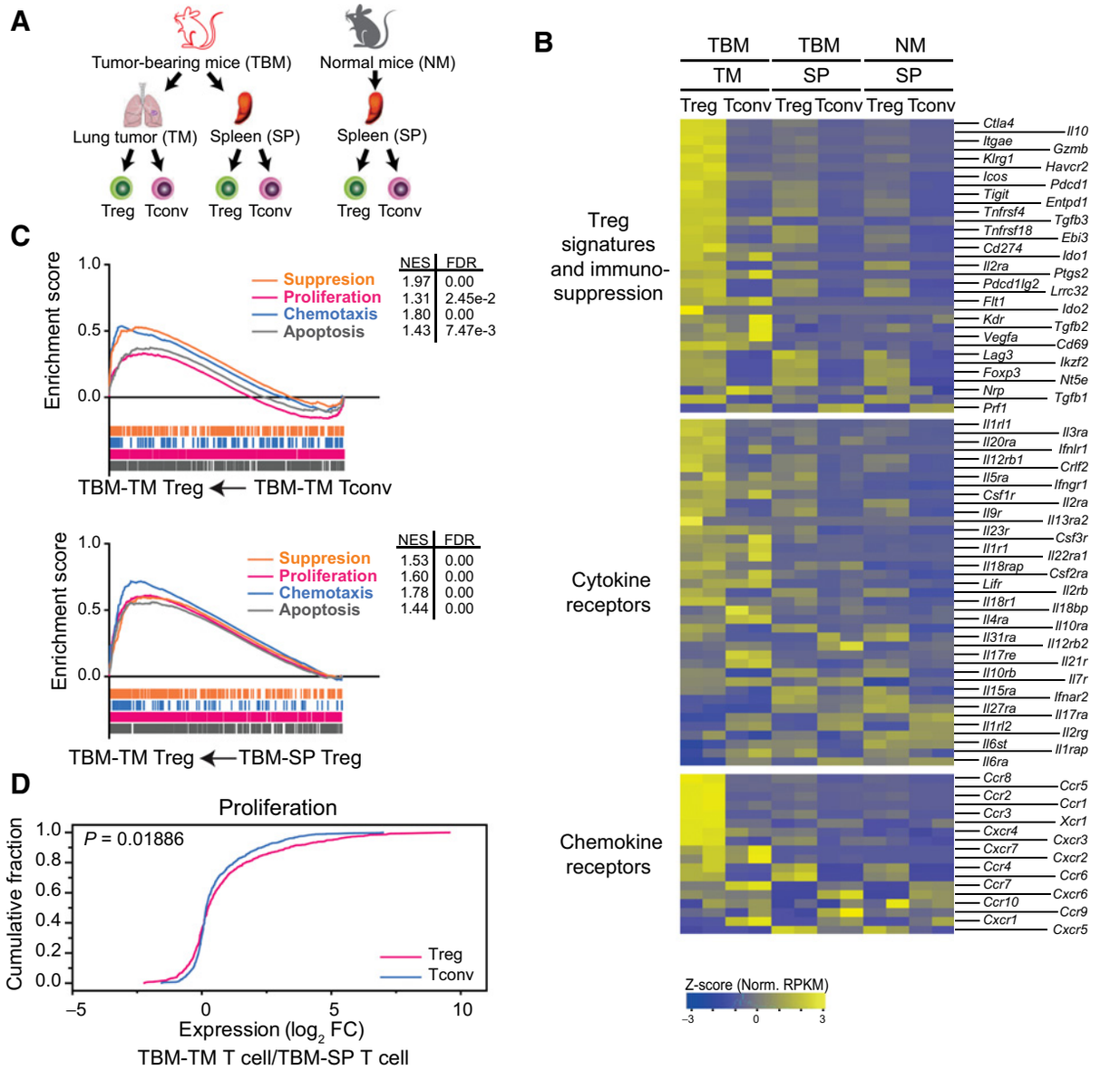

Figure 2.

Comparative transcriptional analysis of Tregs and Tconvs from normal mice and tumor-bearing mice. **A,** Overview of comparative transcriptomic analysis of mouse Tregs and Tconvs using RNA-seq ($n = 2$/group). **B,** Heatmap of gene expression based on z-scores of normalized reads per kilobase million (Norm. RPKM) values for Tregs and Tconvs from tumor-bearing mice (TBM)-TM, TBM-SP, and normal mice (NM)-SP. **C,** GSEA for TBM-TM Tregs compared with TBM-TM Tconvs (top) or with TBM-SP Tregs (bottom). FDR, false discovery rate; NES, normalized enrichment score. **D,** ECDF for expression of proliferation genes based on $\log_2$ FC between TBM-TM Tregs and TBM-SP Tregs (red) and between TBM-TM Tconvs and TBM-SP Tconvs (blue). Kolmogorov–Smirnov two-tailed test was performed for statistical significance.

exposure to antigen. Interestingly, the same clonotype between Tregs and Tconvs was only 1% among tumor-infiltrating Tregs, which was similar to the proportion among normal lung tissue Tregs (Supplementary Fig. S7). Moreover, we observed that the expression profile of tumor-infiltrating rTregs was more similar to that of normal lung tissue Tregs or splenic Tregs in **Fig. 2B**, whereas the expression pattern of tumor-infiltrating aTregs was comparable with that of tumor-infiltrating Tregs in **Fig. 2B** (**Fig. 3E**). Taken together, these results indicated that Tregs in lung tumor were far more proliferative compared with Tregs in normal lung.

Tumor-infiltrating Tregs proliferated more than Tregs under steady-state condition

It has been suggested Treg expansion *in situ* contributes to their accumulation in tumors (6). In addition, we showed that clonally expanded Tregs were enriched in tumor-infiltrating Tregs. To examine whether tumor-infiltrating Tregs proliferated in the TME, BrdU incorporation analysis was performed. Under normal steady-state condition, both Tregs in the spleen and lung incorporated a higher amount of BrdU than Tconvs as described previously (28). In the TME, tumor-infiltrating Tregs proliferated

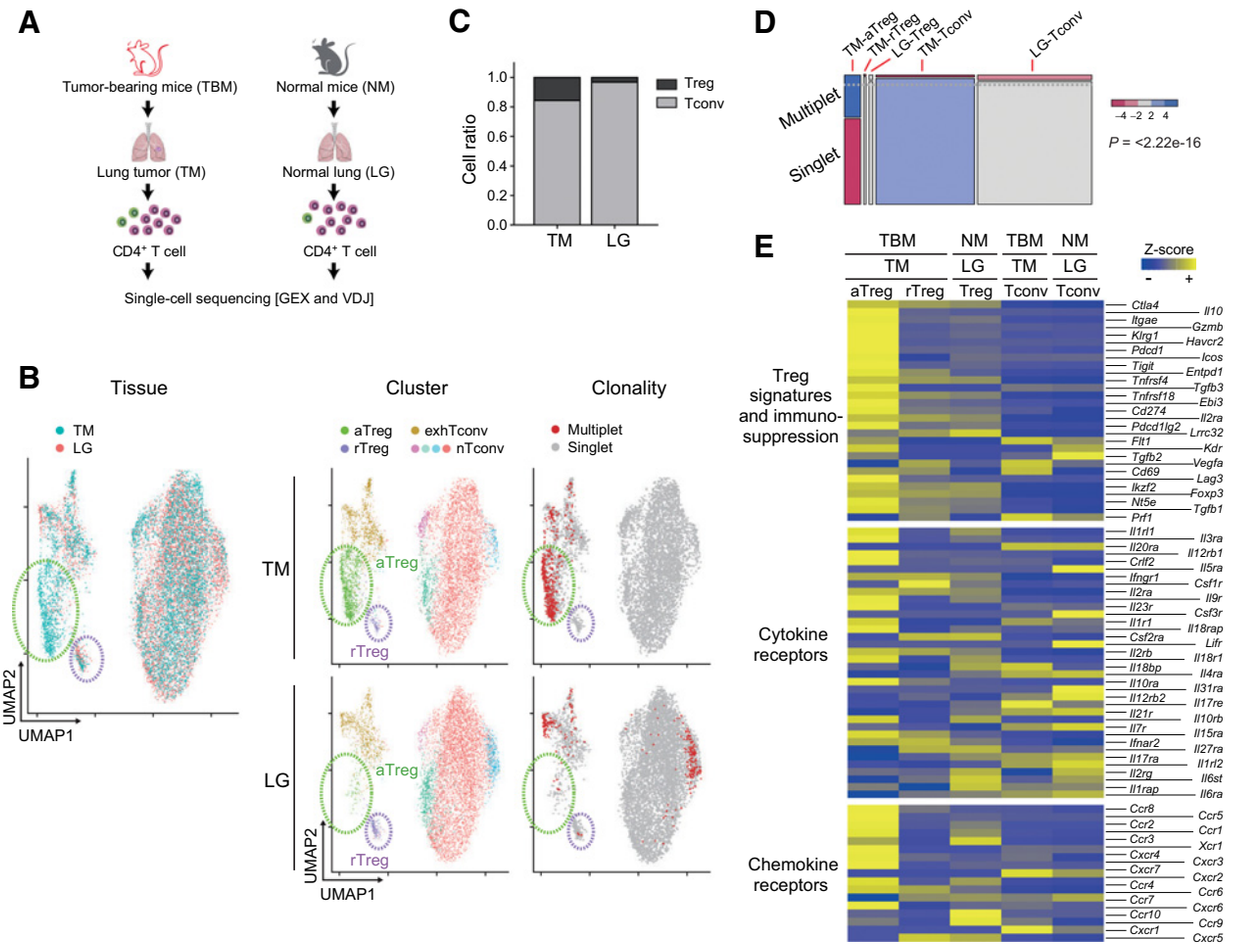

Figure 3.

Comparative scRNA-seq and scTCR-seq analysis of CD4$^+$ T cells from lung tumor and normal lung. **A,** Overview of comparative scRNA-seq and scTCR-seq analysis of CD4$^+$ T cells pooled from lung tumor (TM) of tumor-bearing mice (TBM; $n = 7$) or normal lung (LG) of normal mice (NM; $n = 10$). **B,** UMAP plot of scRNA-seq data by tissue origin (left), cluster (middle), and clonality (right) for TM and LG. **C,** The cumulative barplot for the ratio of Treg and Tconv cell count from TM and LG, respectively. **D,** Mosaic plot comparing cell count between two groups based on clonality (multiplet and singlet) in TM-aTreg, TM-rTreg, LG-Treg (aTreg and rTreg in LG), TM-Tconv, and LG-Tconv. Between the two groups, degree of enrichment or depletion compared with the expected cell count is indicated by blue and red with various intensity for significance level (|Pearson residual|>2: $P < 0.05$, |Pearson residual|>4: $P < 0.0001$). Relative number of cells for each cellular subset is indicated as the area of each rectangle of the mosaic plot. Expected ratio of cell count is indicated as a gray dotted line. Statistical P value for the mosaic plot is shown as χ^2 test. **E,** Heatmap of gene expression from TM-aTreg, TM-rTreg, LG-Treg, TM-Tconv, and LG-Tconv.

much faster than tumor-infiltrating Tconvs and steady-state Tregs (**Fig. 4A** and **B**). Robust proliferation of tumor-infiltrating Tregs was also verified by Ki67 staining (**Fig. 4C** and **D**). These findings indicated a higher turnover rate of Tregs in the TME promotes their accumulation therein. To investigate the apoptotic rates of tumor-infiltrating Tregs, CD4$^+$CD25$^+$ Tregs were stained with Annexin V (AV) and 7-AAD. The numbers of both early apoptotic (AV$^+$7-AAD$^-$) and late apoptotic/dead (AV$^+$7-AAD$^+$) Tregs increased in the TME compared with the lung of normal mice and the spleen of normal mice and tumor-bearing mice (**Fig. 4E** and **F**). Collectively, these data implied that although tumor-infiltrating Tregs displayed a high rate of early and late apoptosis, Tregs in the TME proliferated rapidly enough to overcome the rate of apoptosis of tumor-infiltrating Tregs, resulting in Treg accumulation in the TME.

ST2 was upregulated in tumor-infiltrating Tregs but not in tumor-infiltrating Tconvs

A multistep candidate gene filtration was used to identify the key regulators of Tregs proliferation in the TME (**Fig. 5A**). We hypothesized the key regulators are overexpressed in tumor-infiltrating Tregs. Hence, we filtered the differentially expressed surface protein genes in tumor-infiltrating Tregs versus Tconvs and compared it with five other cellular and tissue contexts (see **Fig. 2A**). A higher level of FC threshold was used to avoid nonspecific targeting of the tumor-infiltrating Tconvs. To obtain high-confidence candidate genes, we generated DEGs based on the consensus of four distinct DEG analysis pipelines (see Methods) and obtained 37 DEGs. We selected 17 genes that express more than 10% of the level of CD4 expression because sufficiently high levels of the drug target molecules was needed to observe the therapeutic effect. To

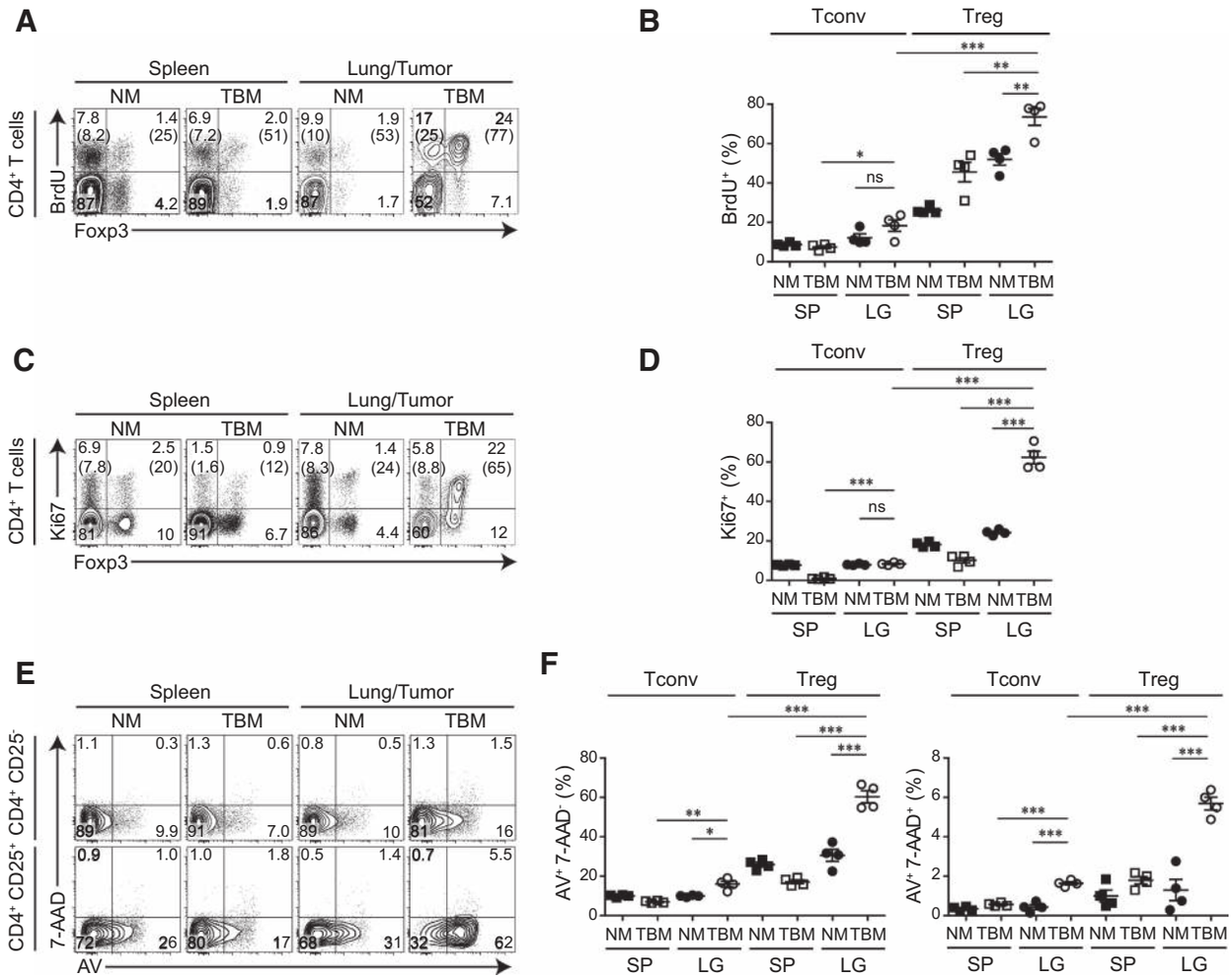

Figure 4.

Preferential proliferation of Tregs in the TME. Representative plots of BrdU incorporation into $CD4^+$ T cells (**A**) and frequency of BrdU-incorporated Tconvs and Tregs (**B**) from tissues of normal mice (NM) and tumor-bearing mice (TBM). Numbers in parentheses indicate the percentage of $BrdU^+$ proliferating cells among Tconvs or Tregs. Representative plots of Ki67 expression in $CD4^+$ T cells (**C**) and frequency of $Ki67^+$ among Tconvs and Tregs (**D**) from the tissues. Numbers in parentheses indicate the percentage of $Ki67^+$ cells among Tconvs or Tregs. **E,** Apoptosis of $CD4^+CD25^-$ Tconvs and $CD4^+CD25^+$ Tregs from the tissues. **F,** Frequency of cells in early and late apoptosis. Data are representative of at least two independent experiments. Results are presented as the mean ± SEM and analyzed by two-tailed unpaired Student *t* test ($n = 4$/group; *, $P < 0.05$; **, $P < 0.01$; ***, $P < 0.001$; ns, not significant). LG, lung; SP, spleen.

specifically target tumor-infiltrating Tregs, we then filtered out the genes that are highly expressed in other immune cell types using the Immgen database (24). We finally obtained three candidate genes, *Il1rl1, Ncmap*, and *Sytl1*, that passed all the filtration criteria (**Fig. 5A**). The expression level of *Ncmap* in other immune cell types could not be tested as this data was not available in the Immgen database. The protein encoded by *Sytl1* had no extracellular domain, whereas that encoded by *Il1rl1* (ST2) contained an extracellular domain based on the UniProtKB/Swiss-Prot database (22). Only *Il1rl1* was annotated as an immune-related gene by GO, and the volcano plot of expression changes exhibited similar expression profiles for *Il1rl1* and other tumor-infiltrating Tregs signature genes (**Fig. 5B**). Thus, we selected *Il1rl1* (ST2) as the candidate gene for further analysis.

We observed the expression of *Il1rl1* significantly correlated with that of genes involved in the proliferation of Tregs isolated from normal and tumor tissues ($P = 6.72E{-}12$; **Fig. 5C**). Consistent with the hypothesis that *Il1rl1* is involved in tumor-infiltrating Tregs proliferation, an increased number of $ST2^+$ Tregs was previously reported in the immune-tolerant environment of the intestine (15). These results suggest ST2 may be a key factor for Treg proliferation in the TME.

We confirmed an enhanced ST2 protein expression in tumor-infiltrating Tregs during tumor progression and nearly 30% of $ST2^+$ tumor-infiltrating Tregs on day 21 in TC-1 tumor model (**Fig. 5D** and **E**). ST2 expression in tumor-infiltrating Tregs was higher than that in tumor-infiltrating Tconvs not only in TC-1 tumor model but also in other tumor models including LLC1 and CT26 (**Fig. 5F** and **G**), indicating high level of ST2 expression is a general feature of tumor-infiltrating Tregs.

In various human cancer types, the *Il1rl1* expression in tumor-infiltrating Tregs was significantly higher than that in Tregs in

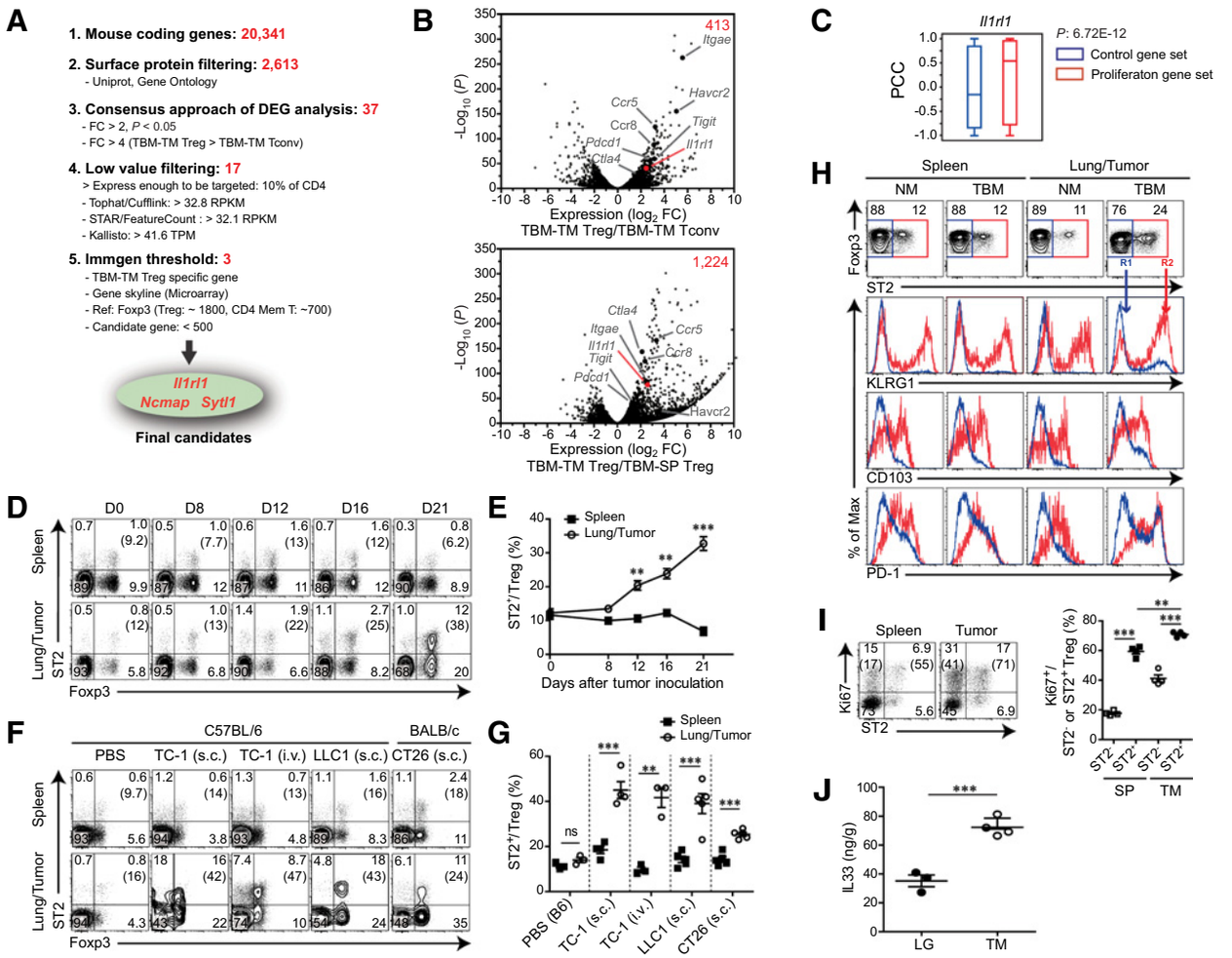

Figure 5.

Identification of ST2 as a key receptor for tumor-infiltrating Treg proliferation. **A,** Multistep gene filtering process to identify key receptors associated with tumor-infiltrating Tregs. RPKM, reads per kilobase million; TPM, transcripts per million. **B,** Volcano plots of gene expression changes in tumor-bearing mice-TM Tregs compared with tumor-bearing mice-TM Tconvs (top) or tumor-bearing mice-SP Tregs (bottom). Total numbers of differentially upregulated genes (FC > 2 and $P < 0.01$) are indicated at the right upper corner. **C,** Boxplots showing distribution of PCC values between *Il1rl1* and proliferation genes or control genes across six Treg samples. Statistical significance of differences between two PCC distributions tested by Wilcoxon rank-sum test. Representative plots of time kinetics of ST2 expression gated on $CD4^+$ T cells from the tissues of normal mice and TC-1 tumor–bearing mice (**D**) and the summarized graph (**E**). Numbers in parentheses indicate the percentage of $ST2^+$ cells among Tregs. Representative plots of ST2 expression gated on $CD4^+$ T cells from the tissues of normal mice and tumor-bearing mice in various tumor models (**F**) and the summarized graph (**G**). **H,** Phenotypic analysis of $ST2^-$ and $ST2^+$ Tregs from the tissues of normal mice and TC-1 tumor–bearing mice on day 16 following tumor inoculation. **I,** Proliferative capacities of $ST2^-$ and $ST2^+$ Tregs from the tissues of tumor-bearing mice on day 16 following tumor inoculation. Numbers in parentheses indicate the percentage of $Ki67^+$ cells among Tconvs or Tregs. **J,** IL33 amount in the normal lung of normal mice and lung tumor of TC-1 tumor–bearing mice on day 8 following tumor inoculation. Data are representative of at least two independent experiments. Results are presented as the mean ± SEM and analyzed by two-tailed unpaired Student *t* test ($n = 4$/group; *, $P < 0.05$; **, $P < 0.01$; ***, $P < 0.001$; ns, not significant). i.v., intravenous; LG, lung; NM, normal mice; s.c., subcutaneous; SP, spleen; TBM, tumor-bearing mice; TM, tumor.

peripheral blood or adjacent normal tissue (Supplementary Fig. S8A; refs. 10, 11). In addition, scRNA-seq data from NSCLC revealed an increased *Il1rl1* in tumor-infiltrating Tregs but not in the blood or adjacent normal tissue Tregs and in tumor-infiltrating Tconvs (Supplementary Fig. S8B; ref. 29). ST2 staining of human Tregs in the blood and tumor tissue obtained from patients with NSCLC confirmed a highly enriched Tregs in tumor tissue and their ST2 expression (Supplementary Fig. S8C). These data indicated ST2 upregulation in Tregs was a distinctive feature of tumor-infiltrating Tregs but not in peripheral tissue Tregs or tumor-infiltrating Tconvs.

To further characterize tumor-infiltrating $ST2^+$ Tregs, we compared $ST2^-$ and $ST2^+$ Tregs in the tissues of normal mice and tumor-bearing mice. As reported in colonic $ST2^+$ Tregs and tissue $ST2^+$ Tregs (15, 30), enhanced expressions of KLRG1 and CD103 were observed in tumor-infiltrating $ST2^+$ Tregs. PD-1 expression in $ST2^+$ tumor-infiltrating Tregs was also higher than that in $ST2^-$ tumor-infiltrating Tregs on day 16 following tumor inoculation, even though the difference was not apparent thereafter (**Fig. 5H**; Supplementary Fig. S9). In addition, Ki67 expression in $ST2^+$ tumor-infiltrating Tregs was significantly higher than in $ST2^-$ tumor-infiltrating Tregs (**Fig. 5I**;

Supplementary Fig. S9B). Similarly, the enhanced Ki67 expression was also observed in human $ST2^+$ tumor-infiltrating Tregs in human NSCLC (Supplementary Fig. S8C). This suggests a proportion of Tregs in the TME exhibits enhanced ST2 expression and strong proliferative capacity.

IL33 binding to ST2 enhances the expression of ST2 through positive feedback loop (14). IL33 expression in the TME was significantly higher than that in the normal lung (**Fig. 5J**). To examine the cellular source of IL33 in the tumor, we performed multiplex immunofluorescence staining. Consistent with the previous reports showing endogenous mouse IL33 expression (31), various cells including $CD31^+$ endothelial cells, $PDPN^+$ epithelial cells, and $CD45^+$ lymphocytes, expressed IL33 in the normal lung (Supplementary Fig. S10A–S10C). We also observed of the other IL33-positive cells in the TME. A previous report in human colon cancer (32) showed that $CD31^+$ endothelial cells expressed IL33 in the TME. However, in our mouse lung tumor model, most of populations were IL33-negative and only small portion of $CD45^+$ cells were IL33-positive (Supplementary Fig. S10B). This discrepancy surrounding the cellular source of IL33 may be due to different tissue or different TME. However, ELISA data showed that IL33 secretion quickly increased in the TME at early time points (day 8) following tumor inoculation and decreased thereafter (Supplementary Fig. S10D). Also, Ki67 level of $ST2^+$ tumor-infiltrating Tregs gradually decreased as lung tumor progresses (Supplementary Fig. S9B). These data suggest that a rapid secretion of IL33 accumulated in the lung rather than upregulated gene expression of IL33 occurs upon an inflammatory signal generated at early stage of lung tumor progression and subsequently, IL33 as an alarmin initiates ST2 upregulation on Tregs in the TME, leading to proliferation of tumor-infiltrating Tregs.

IL33 promoted the expansion of tumor-infiltrating Tregs and accelerated tumor growth

Next, we examined whether *in vitro* cytokine treatment stimulated the expansion of tumor-infiltrating Tregs in the presence of TCR activation. Given tumor-infiltrating Tregs showed upregulation of *Il2ra, Il10ra, Il12rb1*, and *Il1rl1* (**Fig. 2B**), we added the corresponding cytokines to tumor-infiltrating $CD4^+$ T cells. IL33 treatment predominantly increased tumor-infiltrating Tregs (Supplementary Fig. S11). In addition, proliferation of Tregs upon IL33 treatment was greater than that of Tconvs (**Fig. 6A** and **B**). Upon inhibition of ST2, Tregs proliferation was significantly reduced, indicating the IL33-mediated proliferation results from direct interaction with ST2, but, Tconvs proliferation was slightly modulated by IL33 or anti-ST2 antibody treatment. Accordingly, Treg numbers increased upon IL33 treatment and decreased when ST2 was blocked (**Fig. 6C**) or genetically depleted (Supplementary Fig. S12). We also found Tregs proliferation upon IL33 treatment was restricted to ST2-expressing Tregs. Conversely, blocking ST2 decreased the IL33-mediated proliferation of ST2-expressing Tregs (**Fig. 6D** and **E**). Meanwhile, IL33 treatment did not promote the expansion of splenic Tregs from tumor-bearing mice, in which Tregs had limited ST2 expression (Supplementary Fig. S13). This suggests that IL33 promotes the proliferation of $ST2^+$ tumor-infiltrating Tregs through direct interaction with ST2 *in vivo*.

Next, we investigated the potential impact of IL33 on tumor progression *in vivo*. When tumor-bearing mice were treated with IL33 on days 4, 7, and 10 following inoculation, the mice increased number of tumor nodules (**Fig. 6F**). Even single injection with IL33 increased tumor nodules (Supplementary Fig. S14A and S14B). Upon IL33 treatment, frequency of $CD8^+$ T-cell and ratio of $CD8^+$ T cells to Tregs within tumor decreased, but frequency of tumor-infiltrating Tregs significantly increased, suggesting IL33 may play an important role in impairing antitumor immunity (**Fig. 6G**; Supplementary Fig. S14C). Specifically, IL33 promoted the upregulation of Ki67 and ST2 in tumor-infiltrating Tregs *in vivo* (**Fig. 6H** and **I**; Supplementary Fig. S14D and S14E). This resulted in a significantly increased population of the $ST2^+Ki67^+$ tumor-infiltrating Tregs (**Fig. 6I**; Supplementary Fig. S14E). As triggering ST2 signaling by IL33 upregulated ST2 via positive feedback loop, upregulation of Ki67 and ST2 was observed in tumor-infiltrating Tconvs to some extent (**Fig. 6H** and **I**; Supplementary Fig. S14D and S14E).

To test whether these phenotypes were connected to IL33-mediated accelerated tumor growth, we performed *in vitro* suppression assays. As expected, IL33-treated Tregs were more effective at suppressing $CD8^+$ T-cell proliferation than PBS-treated Tregs, when Tregs were administered at 1:1 ratio or 3:1 ratio ($CD8^+$: Treg; **Fig. 6J**). Therefore, IL33 in the TME augments not only Tregs quantity but their function, thus contributing to immune suppression and tumor progression.

ST2 deficiency inhibited the accumulation of Tregs in the TME

We examined whether ST2 deficiency could affect tumor-infiltrating Treg accumulation. In ST2-deficient compared with WT mice, the numbers of tumor nodules and tumor-infiltrating Tregs were significantly reduced (**Fig. 7A** and **B**). A significant decrease of tumor-infiltrating Tregs subsequently led to an increase in the ratio of $CD8^+$ T cells to Tregs within the tumor (**Fig. 7B**) and enhanced IFNγ production in tumor-infiltrating $CD8^+$ T cells (**Fig. 7C**). These results suggest that ST2 signaling plays an essential role in accumulating tumor-infiltrating Tregs and inhibiting $CD8^+$ T cells, thereby contributing to tumor progression.

To confirm whether IL33-mediated Treg proliferation is mediated by ST2 *in vivo*, either WT or ST2-KO mice were treated with IL33 on days 4, 7, and 10 following tumor inoculation (Supplementary Fig. S15A). Consistent with our *in vitro* data, ST2 deficiency did not display Treg accumulation in the TME upon *in vivo* IL33 treatment, resulting in decreased tumor nodules (Supplementary Fig. S15B and S15C). ST2-deficient mice did not also exhibit an enhanced Treg proliferation after *in vivo* IL33 treatment, unlike WT mice (Supplementary Fig. S15D), further supporting that ST2 was critical for IL33-mediated Treg expansion.

To assess whether ST2 deletion in only Tregs could sufficiently inhibit Treg accumulation in the TME, we used coadoptive transfer system, in which Tregs of both WT and ST2-KO were cotransferred along with $CD8^+$ T cells into $Rag2^{-/-}$ mice. The recipient mice were subsequently inoculated with tumors (**Fig. 7D**). In the spleen, there was no difference in the frequency of WT and ST2-KO Tregs. In contrast, within the tumor, the frequency of ST2-KO Tregs markedly decreased compared with that of WT Tregs (**Fig. 7E**). The PD-1–expressing population was significantly less among ST2-KO Tregs than among WT Tregs, implying the association of ST2 with Treg activation (**Fig. 7F**). To test whether ST2-expressing Tregs contributed to an enhanced tumor progression *in vivo*, we performed single-adoptive transfer experiment, in which WT or ST2-KO Tregs were transferred separately (**Fig. 7G**). ST2-KO Treg–transferred mice showed significantly smaller numbers of tumor nodules than WT Treg–transferred mice, indicating that ST2 expression empowered tumor-infiltrating Tregs to suppress antitumor immunity (**Fig. 7H**).

We further tested whether neutralization of ST2 could affect tumor control once tumors were established (**Fig. 7I**). *In vivo* treatment with ST2 antibody decreased tumor nodules (**Fig. 7J**), in which tumor-

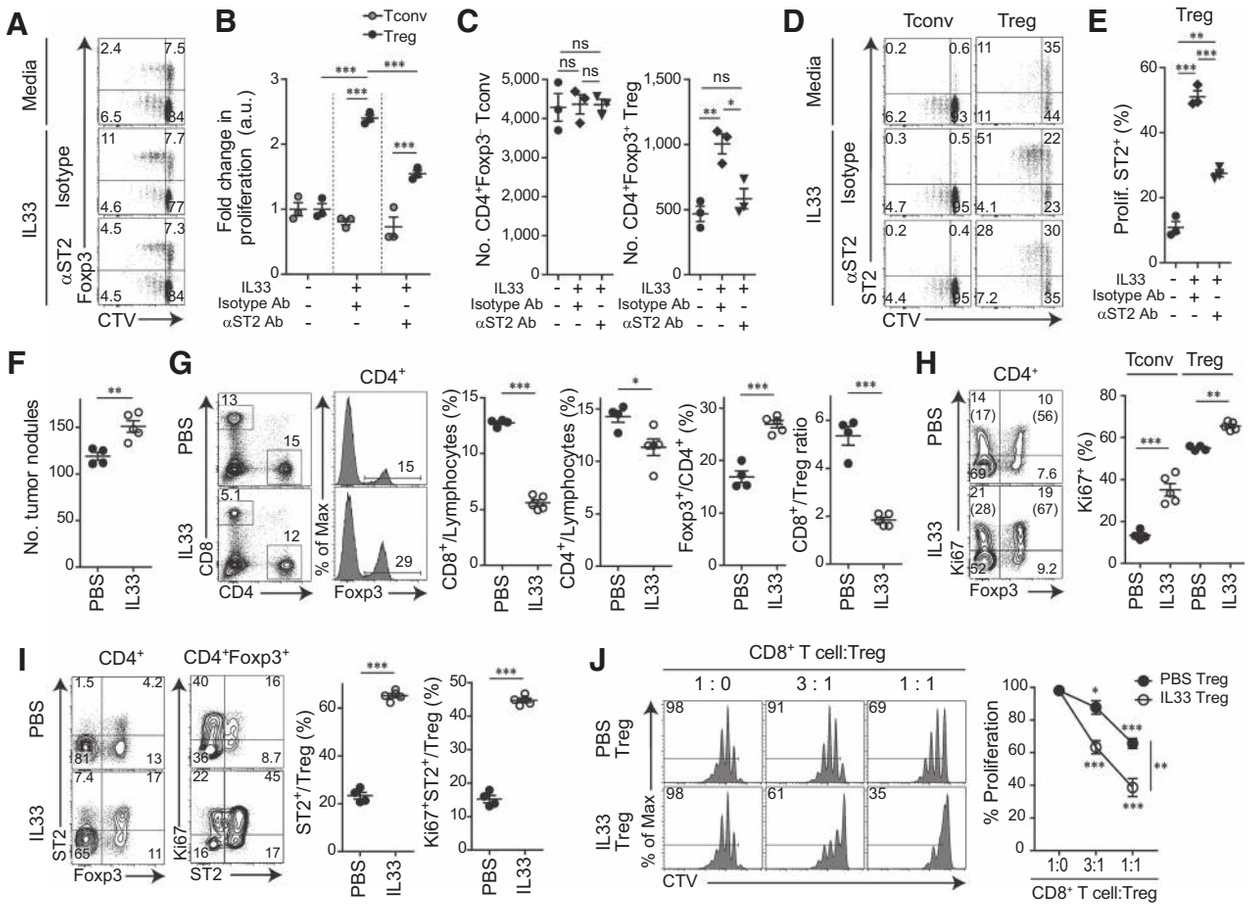

Figure 6.

IL33-mediated expansion of tumor-infiltrating Tregs *in vitro* and *in vivo*. **A–E,** *In vitro* tumor-infiltrating Treg expansion by IL33. **A,** CTV profile showing proliferation versus Foxp3 gated on $CD4^+$ cells. **B,** Fold change in proliferating Tconvs and Tregs treated with IL33 in the absence or presence of ST2-neutralizing antibody. **C,** Absolute number of Tconvs and Tregs. **D,** CTV profile showing proliferation versus ST2 expression. **E,** Frequency of the proliferating (CTV^{low}) $ST2^+$ Tregs. **F–J,** *In vivo* tumor-infiltrating Treg expansion by IL33. Tumor-bearing mice were treated with IL33 on days 4, 7, and 10 and sacrificed on day 13 following tumor inoculation. **F,** Number of tumor nodules in the lung of tumor-bearing mice treated with PBS ($n = 4$) or IL33 ($n = 5$). **G,** Representative plots of the frequency of $CD8^+$ T, $CD4^+$ T, and Tregs and the ratio of $CD8^+$ T and Tregs in the tumor. **H,** Representative plots showing $Ki67^+$ cells among Tconvs and Tregs (left) and frequency of $Ki67^+$ cells among Tconvs or Tregs (right). Numbers in parentheses indicate the percentage of $Ki67^+$ cells among Tconvs or Tregs (left). **I,** Representative plots showing Foxp3 versus ST2 among $CD4^+$ T cells and ST2 versus Ki67 among Tregs (left). Frequency of $ST2^+$ cells and $Ki67^+ST2^+$ cells among Tregs (right). **J,** Representative plots of CTV-labeled $CD8^+$ T cells following 72 hours of culture with or without PBS and IL33 Tregs at different ratio. Numbers at the top left of each histogram indicate the percentage of CTV-labeled $CD8^+$ T cells ($n = 3$/group). Data are representative of at least three independent experiments. Results are presented as the mean ± SEM. Statistical significance was determined by one-way ANOVA with Bonferroni *post hoc* test (**A–E**; $n = 3$/group) and unpaired Student *t* test (**F–J**; *, $P < 0.05$; **, $P < 0.01$; ***, $P < 0.001$; ns, not significant).

infiltrating Tregs exhibited reduced Ki67 and ST2 expression (**Fig. 7K**), indicating that ST2 was critical for tumor-infiltrating Treg proliferation.

Taken together, these data indicated IL33/ST2 axis–mediated intrinsic signaling in Tregs promoted their proliferation, which was one of the critical pathways for the preferential accumulation of Tregs in the TME, thus contributing to the inhibition of antitumor immune response and subsequent tumor progression.

Discussion

In this study, we investigated the molecular mechanisms by which Tregs accumulate in the TME. Our transcriptome analysis of tumor-infiltrating Tregs revealed functional molecules and cellular processes involved in Treg accumulation in the TME. Recent reports human tumor-infiltrating Tregs exhibit a different gene expression compared with blood Tregs or tumor-infiltrating Tconvs support the concept for TME-dependent changes of tumor-infiltrating Tregs (10, 33). In particular, the genes involved in proliferation, cell cycle, and chemotaxis were significantly enriched in tumor-infiltrating Tregs.

One possible explanation for the high density of Tregs in the TME is that the enhanced proliferation of tumor-infiltrating Tregs leads to their accumulation. Using multistep candidate gene-filtering process, we identified ST2 was one of significantly upregulated receptors in tumor-infiltrating Tregs. Tregs observed in adipose tissue and skin express high level of ST2 as determined by methylome and transcriptome patterns (30). In addition, ST2 expression was required for

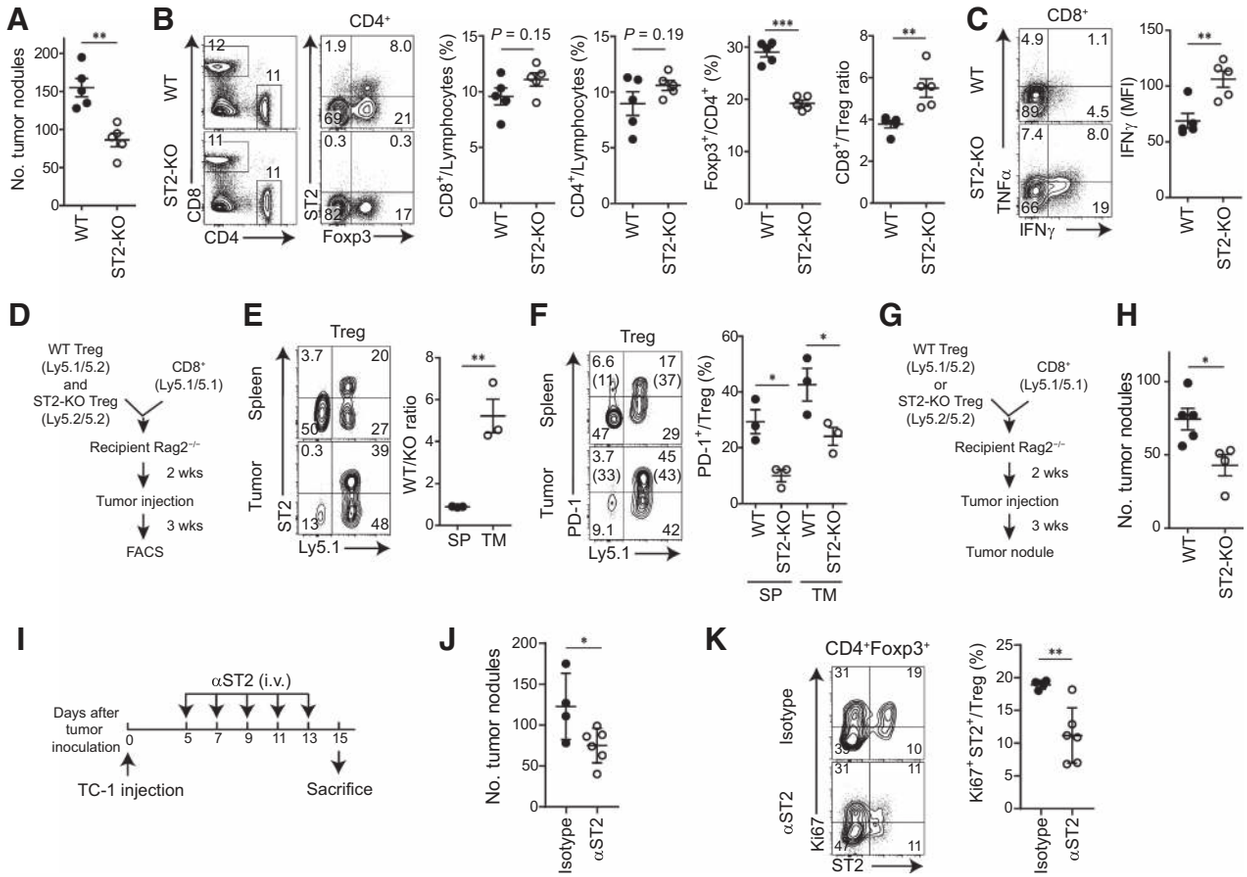

Figure 7.

ST2 deficiency–mediated suppression of tumor progression and tumor-infiltrating Treg accumulation. **A,** Number of tumor nodules in the lung of tumor-bearing WT or ST2-deficient mice (n = 5/group). **B,** Representative plots for the frequency of $CD8^+$ T, $CD4^+$ T, and Tregs and the ratio of $CD8^+$ T and Tregs in tumors. **C,** Representative plots and median fluorescence intensity (MFI) of IFNγ among $CD8^+$ T cells. **D–F,** *in vivo* ST2-KO Treg proliferation in the TME. **D,** Experimental scheme. **E,** Ratio of WT and ST2-KO Tregs in the tissues (n = 3/group). **F,** Expression of PD-1 in WT and ST2-KO Tregs in the tissues. **G** and **H,** *in vivo* functionality of ST2-KO Tregs. **G,** Experimental scheme. **H,** Number of tumor nodules from tumor-bearing mice with adoptively transferred WT Tregs (n = 5) or ST2-KO Tregs (n = 4). **I–K,** *In vivo* treatment of ST2-neutralizing antibody. **I,** Experimental scheme. i.v., intravenous. **J,** Number of tumor nodules from tumor-bearing mice treated with isotype (n = 4) or anti-ST2 (n = 6). **K,** Representative plot and frequency of proliferating $ST2^+$ Tregs in the tumor upon anti-ST2 treatment. Data are representative of two independent experiments. Results are the mean ± SEM, and statistical significance was determined by two-tailed unpaired Student t test (*, $P < 0.05$; **, $P < 0.01$; ***, $P < 0.001$).

colonic or adipose Treg-specific expansion (15, 16, 34). While IL33 promotes tumor not only in mouse tumor models (35, 36) but also in clinical tumor patients (37, 38), few studies reported regarding the direct role of IL33 in tumor-infiltrating Treg expansion. Here, we demonstrated both *in vitro*– and *in vivo*–treated IL33 showed a growth factor-like effect on the expansion of tumor-infiltrating Tregs. IL33-dependent preferential proliferation of Tregs in the TME might contribute to the inhibition of tumor antigen–specific T cell responses, thereby promoting tumor progression. Indeed, IL33 treatment accelerates tumor growth in two different cancer models, 4T1 and CT26 (35, 39). However, we cannot exclude the possibility of Treg-independent mechanism for IL33-mediated tumor progression considering not only the ST2 expression by various types of immune cells but also the direct and indirect effects of IL33 contribute to this process (40). More comprehensive studies using ST2 conditional knockout in various immune cell types might address this issue.

IL33 increased in the TME at the early stage of tumor progression, which suggests a rapid IL33 secretion induces ST2 upregulation on tumor-infiltrating Tregs via a positive feedback loop, resulting in IL33/ST2-dependent vigorous proliferation. Although IL33/ST2 signaling remains to be explored, blocking the IL33/ST2 axis on tumor-infiltrating Tregs could be a potential therapeutic strategy. Indeed, ST2 blockade controlled tumor burden in our study and IL33 blockade suppressed tumor growth in another preclinical model (41). In addition, soluble form of ST2 (sST2) as a decoy receptor led to tumor growth inhibition by modulating TME (42). More convincingly, our data using ST2-KO Tregs clearly demonstrated that ST2 expression in Tregs was critical in their proliferation and accumulation in the TME. One interesting observation was that PD-1 is expressed much less in ST2-KO Tregs compared with WT Tregs, suggesting ST2 signaling in Tregs associated with an activation pathway.

Second possibility for Treg enrichment is the selective trafficking of Tregs into the TME. Tumor cells and tumor-associated macrophages secrete CCL22 to facilitate CCR4-expressing Tregs in human ovarian cancer (43). CCR8 was upregulated in tumor-infiltrating Tregs in breast cancer, colorectal carcinoma, melanoma, and lung

adenocarcinoma, suggesting CCR8 as a potential therapeutic target for Treg modulation (10, 11). Blocking multiple chemokine receptors may block more efficiently Treg migration into the TME due to redundancy between modules of chemokine ligand/receptors. For example, blocking both CCL2 and CCL12 in combination with the Ad.E7 vaccine significantly decreased tumor-infiltrating Treg frequency and augmented antitumor immunity (44). Combination of CCL1 blocker and CpG-ODN resulted in not only reduction of tumor-infiltrating Tregs but also complete rejection of the tumor (45).

Another possibility for Treg enrichment is conversion of Tconvs to Tregs in the TME. On the basis of the observation that Tregs usually express a high Nrp1, most tumor-infiltrating Tregs are peripherally derived from Tconvs (46). However, it now appears that Nrp1 may not be an appropriate marker to distinguish Treg origin (37). As shown in Supplementary Fig. S7, tumor-infiltrating Tregs and tumor-infiltrating Tconvs shared only 1% of TCR repertoire, which suggests tumor-infiltrating Tregs are dominantly derived from pre-existing Tregs rather than conversion from Tconvs. Regarding the origin of tumor-infiltrating Tregs, previous studies support our observation. Epigenetic (47) and TCR repertoire analysis (48) suggest tumor-infiltrating Tregs originate from naturally occurring Tregs. In addition, tumor antigen–specific Tregs are developed in the thymus in an autoimmune regulator (Aire)–dependent manner (49).

The major mechanism underlying immune suppression by tumor-infiltrating Tregs has not yet been clarified. Analysis of gene sets found molecules related to immune suppression were enhanced in the TME. This finding provides an intriguing hypothesis that immune checkpoint antibodies given to patients with cancer might bind more strongly to tumor-infiltrating Tregs than to tumor-infiltrating Tconvs. In accordance with this hypothesis, anti–CTLA-4 given to melanoma patients bound to CTLA4 expressed by Tregs and induced the depletion of CTLA-4–expressing Tregs (50, 51). Thus, the action mechanism of immune checkpoint inhibitors might be mediated by functional neutralization and/or depletion of the corresponding immune checkpoint–expressing Tregs in the TME.

In conclusion, our study delineated the cellular processes and the key molecule involved in Treg accumulation in the TME. Furthermore, our work provided novel insights and strategies for therapeutic targeting of tumor-infiltrating Tregs via modulating the IL33/ST2 axis.

Disclosure of Potential Conflicts of Interest

J. Son reports a patent for "Compositions and Methods for Treatment of Cancers" pending. J.-W. Cho reports a patent for "Compositions and Methods for Treatment of Cancers" pending. J. Moon reports a patent for "Compositions and Methods for Treatment of Cancers" pending. S. Park reports a patent for "Compositions and Methods for Treatment of Cancers" pending. I. Lee reports a patent for "Compositions and Methods for Treatment of Cancers" pending. S.-J. Ha reports a patent for "Compositions and Methods for Treatment of Cancers" pending. No potential conflicts of interest were disclosed by the other authors.

Authors' Contributions

J. Son: Conceptualization, data curation, formal analysis, funding acquisition, validation, investigation, methodology, writing–original draft, writing–review and editing. **J.-W. Cho:** Conceptualization, resources, data curation, software, formal analysis, validation, investigation, methodology, writing–original draft, writing–review and editing. **H.J. Park:** Conceptualization, data curation, formal analysis, investigation, methodology. **J. Moon:** Data curation, formal analysis, validation, investigation, visualization, methodology, writing–original draft. **S. Park:** Resources, data curation, formal analysis, validation, investigation. **H. Lee:** Resources, investigation, methodology. **J. Lee:** Resources, data curation, investigation, methodology. **G. Kim:** Resources, formal analysis, investigation, methodology. **S.-M. Park:** Resources, formal analysis, investigation, methodology. **S.A. Lira:** Resources, methodology. **A.N. Mckenzie:** Resources, methodology. **H.Y. Kim:** Conceptualization, resources, methodology. **C.Y. Choi:** Conceptualization, resources, methodology. **Y.T. Lim:** Conceptualization, resources, methodology. **S.Y. Park:** Resources, investigation, methodology. **H.R. Kim:** Conceptualization, resources, data curation, funding acquisition, investigation, methodology, writing–original draft. **S.-H. Park:** Conceptualization, resources, investigation, methodology. **E.-C. Shin:** Conceptualization, resources, investigation, methodology. **I. Lee:** Conceptualization, data curation, software, formal analysis, supervision, funding acquisition, validation, investigation, visualization, writing–original draft, project administration, writing–review and editing. **S.-J. Ha:** Conceptualization, resources, data curation, software, formal analysis, supervision, funding acquisition, validation, investigation, visualization, methodology, writing–original draft, project administration, writing–review and editing.

Acknowledgments

This study was supported by a National Research Foundation of Korea (NRF) grant funded by the Korea government (MSIT; 2012H1A2A1016220, to J. Son; 2017R1A5A1014560, 2018M3A9H3024850, 2018R1A2A1A05076997, and 2019M3A9B6065221, to S-.J. Ha; 2019M3A9B6065192 and 2018R1A5A2025079, to I. Lee; and 2019M3A9B6065231, to H.R. Kim). J. Son, J.-W. Cho, H.J. Park, J. Moon, and S. Park are fellowship awardees by the BK21 PLUS program.

The costs of publication of this article were defrayed in part by the payment of page charges. This article must therefore be hereby marked *advertisement* in accordance with 18 U.S.C. Section 1734 solely to indicate this fact.

Received October 24, 2019; revised July 8, 2020; accepted August 27, 2020; published first September 2, 2020.

References

1. Beyer M, Schultze JL. Regulatory T cells in cancer. Blood 2006;108:804–11.
2. Liu C, Workman CJ, Vignali DA. Targeting regulatory T cells in tumors. FEBS J 2016;283:2731–48.
3. Colombo MP, Piconese S. Regulatory-T-cell inhibition versus depletion: the right choice in cancer immunotherapy. Nat Rev Cancer 2007;7:880–7.
4. Teng MW, Ngiow SF, von Scheidt B, McLaughlin N, Sparwasser T, Smyth MJ. Conditional regulatory T-cell depletion releases adaptive immunity preventing carcinogenesis and suppressing established tumor growth. Cancer Res 2010;70:7800–9.
5. Tanaka A, Sakaguchi S. Regulatory T cells in cancer immunotherapy. Cell Res 2017;27:109–18.
6. Zou W. Regulatory T cells, tumour immunity and immunotherapy. Nat Rev Immunol 2006;6:295–307.
7. Mailloux AW, Young MR. Regulatory T-cell trafficking: from thymic development to tumor-induced immune suppression. Crit Rev Immunol 2010;30:435–47.
8. Ondondo B, Jones E, Godkin A, Gallimore A. Home sweet home: the tumor microenvironment as a haven for regulatory T cells. Front Immunol. 2013;4:197.
9. Nagarsheth N, Wicha MS, Zou W. Chemokines in the cancer microenviroenvironment and their relevance in cancer immunotherapy. Nat Rev Immunol 2017;17:559–72.
10. De Simone M, Arrigoni A, Rossetti G, Gruarin P, Ranzani V, Politano C, et al. Transcriptional landscape of human tissue lymphocytes unveils uniqueness of tumor-infiltrating T regulatory cells. Immunity 2016;45:1135–47.
11. Plitas G, Konopacki C, Wu K, Bos PD, Morrow M, Putintseva EV, et al. Regulatory T cells exhibit distinct features in human breast cancer. Immunity 2016;45:1122–34.
12. Moo-Young TA, Larson JW, Belt BA, Tan MC, Hawkins WG, Eberlein TJ, et al. Tumor derived TGF-Beta mediates conversion of CD4+ Foxp3+ regulatory T cells in a murine model of pancreas cancer. J Immunother 2009;32:12–21.
13. Liew FY, Girard J-P, Turnquist HR. Interleukin-33 in health and disease. Nat Rev Immunol 2016;16:676–89.
14. Peine M, Marek RM, Löhning M. IL33 in T cell differentiation, function, and immune homeostasis. Trends Immunol 2016;37:321–33.

15. Schiering C, Krausgruber T, Chomka A, Frohlich A, Adelmann K, Wohlfert EA, et al. The alarmin IL33 promotes regulatory T-cell function in the intestine. Nature 2014;513:564–8.
16. Kolodin D, van Panhuys N, Li C, Magnuson AM, Cipolletta D, Miller CM, et al. Antigen- and cytokine-driven accumulation of regulatory T cells in visceral adipose tissue of lean mice. Cell Metab 2015;21:543–57.
17. Wasmer MH, Krebs P. The role of IL33-dependent inflammation in the tumor microenvironment. Front Immunol 2017;7:682.
18. Rosenbloom KR, Armstrong J, Barber GP, Casper J, Clawson H, Diekhans M, et al. The UCSC Genome Browser database: 2015 update. Nucleic Acids Res 2015;43:D670–81.
19. Dobin A, Davis CA, Schlesinger F, Drenkow J, Zaleski C, Jha S, et al. STAR: ultrafast universal RNA-seq aligner. Bioinformatics 2013;29:15–21.
20. Liao Y, Smyth GK, Shi W. featureCounts: an efficient general purpose program for assigning sequence reads to genomic features. Bioinformatics 2014;30:923–30.
21. Pruitt KD, Harrow J, Harte RA, Wallin C, Diekhans M, Maglott DR, et al. The consensus coding sequence (CCDS) project: identifying a common protein-coding gene set for the human and mouse genomes. Genome Res 2009;19:1316–23.
22. Famiglietti ML, Estreicher A, Gos A, Bolleman J, Géhant S, Breuza L, et al. Genetic variations and diseases in UniProtKB/Swiss-Prot: the ins and outs of expert manual curation. Hum Mutat 2014;35:927–35.
23. Ashburner M, Ball CA, Blake JA, Botstein D, Butler H, Cherry JM, et al. Gene ontology: tool for the unification of biology. The Gene Ontology Consortium. Nat Genet 2000;25:25–9.
24. Heng TS, Painter MW. Immunological Genome Project Consortium. The Immunological Genome Project: networks of gene expression in immune cells. Nat Immunol 2008;9:1091–4.
25. Delpoux A, Yakonowsky P, Durand A, Charvet C, Valente M, Pommier A, et al. TCR signaling events are required for maintaining CD4 regulatory T cell numbers and suppressive capacities in the periphery. J Immunol 2014;193:5914–23.
26. Subramanian A, Tamayo P, Mootha VK, Mukherjee S, Ebert BL, Gillette MA, et al. Gene set enrichment analysis: a knowledge-based approach for interpreting genome-wide expression profiles. Proc Natl Acad Sci U S A 2005;102:15545–50.
27. Butler A, Hoffman P, Smibert P, Papalexi E, Satija R. Integrating single-cell transcriptomic data across different conditions, technologies, and species. Nat Biotechnol 2018;36:411–20.
28. Shen CR, Yang WC, Chen HW. The fate of regulatory T cells: survival or apoptosis. Cell Mol Immunol 2014;11:11–3.
29. Guo X, Zhang Y, Zheng L, Zheng C, Song J, Zhang Q, et al. Global characterization of T cells in non-small-cell lung cancer by single-cell sequencing. Nat Med 2018;24:978–85.
30. Delacher M, Imbusch CD, Weichenhan D, Breiling A, Hotz-Wagenblatt A, Träger U, et al. Genome-wide DNA-methylation landscape defines specialization of regulatory T cells in tissues. Nat Immunol 2017;18:1160–72.
31. Pichery M, Mirey E, Mercier P, Lefrancais E, Dujardin A, Ortega N, et al. Endogenous IL33 is highly expressed in mouse epithelial barrier tissues, lymphoid organs, brain, embryos, and inflamed tissues: in situ analysis using a novel IL33–LacZ gene trap reporter strain. J Immunol 2012;188:3488–95.
32. Fang M, Li Y, Huang K, Qi S, Zhang J, Zgodzinski W, et al. IL33 promotes colon cancer cell stemness via JNK activation and macrophage recruitment. Cancer Res 2017;77:2735–45.
33. Panduro M, Benoist C, Mathis D. Tissue tregs. Annu Rev Immunol 2016;34:609–33.
34. Vasanthakumar A, Moro K, Xin A, Liao Y, Gloury R, Kawamoto S, et al. The transcriptional regulators IRF4, BATF and IL33 orchestrate development and maintenance of adipose tissue–resident regulatory T cells. Nat Immunol 2015;16:276–85.
35. Zhou Y, Ji Y, Wang H, Zhang H, Zhou H. IL33 promotes the development of colorectal cancer through inducing tumor-infiltrating ST2L+ regulatory T cells in mice. Technol Cancer Res Treat 2018;17:1533033818780091.
36. Pastille E, Wasmer MH, Adamczyk A, Vu VP, Mager LF, Phuong NNT, et al. The IL33/ST2 pathway shapes the regulatory T cell phenotype to promote intestinal cancer. Mucosal Immunol 2019;12:990–1003.
37. Wen YH, Lin HQ, Li H, Zhao Y, Lui VWY, Chen L, et al. Stromal interleukin-33 promotes regulatory T cell-mediated immunosuppression in head and neck squamous cell carcinoma and correlates with poor prognosis. Cancer Immunol Immunother 2019;68:221–32.
38. Cui G, Li Z, Ren J, Yuan A. IL33 in the tumor microenvironment is associated with the accumulation of FoxP3-positive regulatory T cells in human esophageal carcinomas. Virchows Arch 2019;475:579–86.
39. Jovanovic IP, Pejnovic NN, Radosavljevic GD, Pantic JM, Milovanovic MZ, Arsenijevic NN, et al. Interleukin-33/ST2 axis promotes breast cancer growth and metastases by facilitating intratumoral accumulation of immunosuppressive and innate lymphoid cells. Int J Cancer 2014;134:1669–82.
40. Matta BM, Lott JM, Mathews LR, Liu Q, Rosborough BR, Blazar BR, et al. IL33 is an unconventional Alarmin that stimulates IL-2 secretion by dendritic cells to selectively expand IL33R/ST2+ regulatory T cells. J Immunol 2014;193:4010–20.
41. Wang K, Shan S, Yang Z, Gu X, Wang Y, Wang C, et al. IL33 blockade suppresses tumor growth of human lung cancer through direct and indirect pathways in a preclinical model. Oncotarget 2017;8:68571–82.
42. Akimoto M, Maruyama R, Takamaru H, Ochiya T, Takenaga K. Soluble IL33 receptor sST2 inhibits colorectal cancer malignant growth by modifying the tumour microenvironment. Nat Commun 2016;7:13589.
43. Curiel TJ, Coukos G, Zou L, Alvarez X, Cheng P, Mottram P, et al. Specific recruitment of regulatory T cells in ovarian carcinoma fosters immune privilege and predicts reduced survival. Nat Med 2004;10:942–9.
44. Fridlender ZG, Buchlis G, Kapoor V, Cheng G, Sun J, Singhal S, et al. CCL2 blockade augments cancer immunotherapy. Cancer Res 2010;70:109–18.
45. Hoelzinger DB, Smith SE, Mirza N, Dominguez AL, Manrique SZ, Lustgarten J. Blockade of CCL1 inhibits T regulatory cell suppressive function enhancing tumor immunity without affecting T effector responses. J Immunol 2010;184:6833–42.
46. Weiss JM, Bilate AM, Gobert M, Ding Y, de Lafaille MAC, Parkhurst CN, et al. Neuropilin 1 is expressed on thymus-derived natural regulatory T cells, but not mucosa-generated induced Foxp3+ T reg cells. J Exp Med 2012;209:1723–42.
47. Waight JD, Takai S, Marelli B, Qin G, Hance KW, Zhang D, et al. Cutting edge: epigenetic regulation of Foxp3 defines a stable population of CD4+ regulatory T cells in tumors from mice and humans. J Immunol 2015;194:878–82.
48. Savage PA, Leventhal DS, Malchow S. Shaping the repertoire of tumor-infiltrating effector and regulatory T cells. Immunol Rev 2014;259:245–58.
49. Malchow S, Leventhal DS, Nishi S, Fischer BI, Shen L, Paner GP, et al. Aire-dependent thymic development of tumor-associated regulatory T cells. Science 2013;339:1219–24.
50. Selby MJ, Engelhardt JJ, Quigley M, Henning KA, Chen T, Srinivasan M, et al. Anti-CTLA-4 antibodies of IgG2a isotype enhance antitumor activity through reduction of intratumoral regulatory T cells. Cancer Immunol Res 2013;1:32–42.
51. Simpson TR, Li F, Montalvo-Ortiz W, Sepulveda MA, Bergerhoff K, Arce F, et al. Fc-dependent depletion of tumor-infiltrating regulatory T cells co-defines the efficacy of anti–CTLA-4 therapy against melanoma. J Exp Med 2013;210:1695–710.